Considerations of Sample Thickness and Detector Placement in Intensity Limited Polychromatic X-Ray Diffraction Experiments

Authors:

John Andrew Copley[a], Benjamin Ellyson[a], Jonah Klemm-Toole[a], Jinling Gao[b], Nesredin Kedir[c], Cody Kirk[c], Wayne Chen[b], Niranjan Parabd[e], Tao Sun[f], Kamel Fezzaa[d], Kester Clarke[a] and Amy Jean Clarke[a*]

[a]Metallurgical and Materials Engineering, Colorado School of Mines, Golden, CO, 80401, United States

[b]School of Aeronautics and Astronautics, Purdue University, West Lafayette, IN, 47907, United States

[c]School of Materials Engineering, Purdue University, West Lafayette, IN, 47907, United States

[d]X-Ray Science Division, Argonne National Laboratory, Lemont, IL, 60439, United States

[e] Intel Co., Hillsboro, OR, 97124, United States

[f]Materials Science and Engineering, University of Virginia, Charlottesville, VA, 22904, United States

* Indicates corresponding author

Correspondence email: amyclarke@mines.edu

Acknowledgements This work was supported by the U.S. Department of the Navy, Office of Naval Research under ONR award number N00014-18-1-2567. Any opinions, findings, and conclusions or recommendations expressed in this material are those of the author(s) and do not necessarily reflect the views of the Office of Naval Research. JKT and KDC acknowledge support by the Center for Advanced Non-Ferrous Structural Alloys (CANFSA), a National Science Foundation Industry/University Cooperative Research Center (I/UCRC) [Award No. 1624836], at the Colorado School of Mines (Mines). The authors gratefully acknowledge Gus Becker, Christopher Finfrock, Yaofeng Guo, Chloe Johnson, Brian Milligan, Connor Rietema, Alec Saville, and Doug Smith at Mines for their help performing these experiments. Additionally, the authors would like to thank the reviewers who made insightful and helpful comments that resulted in the improvement of this paper during the review process. This research used resources of the Advanced Photon Source, a U.S. Department of Energy (DOE) Office of Science User Facility operated for the DOE Office of Science by Argonne National Laboratory under Contract No. DE-AC02-06CH11357; synchrotron x-ray data were collected at the Sector 32-ID beamline.

Abstract

Synchrotron light sources enable high rate, time resolved, simultaneous X-ray diffraction and imaging experiments. For intensity limited experiments involving time resolved diffraction, monochromacity may be sacrificed in favor of higher intensity polychromatic beams for increased time resolution. In these instances, consideration must be paid to experimental design parameters, such as sample thickness and detector placement, that can be of special importance in experiments using so called “pink” beam X-rays. To evaluate these considerations, the MATLAB program High Speed Polychromatic X-Ray Diffraction (HiSPoD) and other programs like it, serve as a powerful tool for processing and interpreting data. This work focuses on the use of HiSPoD as a preparatory tool for improving the results of diffraction performed using polychromatic synchrotron x-rays, with a specific focus on using HiSPoD to evaluate sample geometries and detector positions to improve data acquisition and the interpretability of collected diffraction results during high strain rate deformation. To this end, a case study of a metastable multi-principal-element-alloy (MPEA) that undergoes phase transition during high-rate deformation is provided to illustrate the difference between diffraction results for experiments where the effects are and are not taken into consideration during prior planning.

Keywords: X-ray diffraction, In-situ measurement, High-strain-rate deformation

1. Introduction

Synchrotron light sources provide the capability to perform highly informative and unique experiments as a result of their high intensity, tunable X-ray energies and ability to perform ultra-fast imaging and diffraction experiments [1–3]. Synchrotron light sources may be used for imaging (microscopy), absorption spectroscopy, and diffraction experiments [1]. For the latter, the beam may be monochromatized by use of mirrorsor diffraction through a perfect crystal to improve the reciprocal-space resolution of the collected diffraction patterns [4]. Flux- or intensity-limited experiments, such as high-rate-time-resolved diffraction, may not benefit from the use of a highly monochromatic beam, being unable to collect sufficient diffracted intensity with a short detector gating time to produce an interpretable diffraction pattern. In these instances, use of a higher intensity polychromatic beam generated by an undulator may be preferable, even at the expense of the resolution of the diffraction patterns. Due to complications

introduced by the use of a polychromatic beam and the limited time available to users of synchrotron light sources, preparation by means of modelling experimental parameters enables users to minimize time spent in finding desirable experimental parameters on-site.

HiSPoD or High Speed Polychromatic x-ray Diffraction is a MATLAB based program developed at the Advanced Photon Source (APS) at Argonne National Laboratory for the purposes of processing and interpreting x-ray diffraction data collected using a polychromatic beam [5]. Specifically, HiSPoD was developed for diffraction experiments at beamline 32-ID of the APS, which is equipped with a miniaturized pressure bar and gas-gun for high-rate deformation experiments [6, 7]. These experiments occur in time frames of tens of microseconds or less, and thus require high X-ray fluxes to generate sufficient diffracted intensity for interpretable diffraction results [5]. HiSPoD includes the capability to produce simulated diffraction patterns, when provided information about detector position, the energy intensity spectrum, the sample crystal structure and its allowed peaks and their relative intensities [5]. Generally, this information is used to locate the beam center (i.e. transmitted beam position) using a built-in functionality. Locating the beam center allows for integration of the collected area patterns into more conventional $2\theta\ vs.$ Intensity plots. Additionally, because most experiments are performed in transmission mode, HiSPoD includes the capability to modify the energy spectrum used by the program to simulate the X-ray diffraction pattern by the fraction of intensity transmitted through the sample. While results in this work are generated using HiSPoD, evaluation of detector placement and sample geometry effects could be made using any software with similar capabilities as HiSPoD

There are several important considerations in selecting a sample thickness for use in a transmission X-ray diffraction experiment using a polychromatic beam: those favoring thicker samples and those favoring thin samples. Samples with high thickness are generally more practical to produce and easier to work with. Additionally, given a fixed grain size, thicker samples will contain more grains and are more likely to produce full rings rather than “spotty” rings in the area diffraction patterns relative to a thin sample. Factors favoring thin samples generally relate to the polychromatic nature of the beam used for high-rate time-resolved diffraction experiments and consideration of the material under investigation. This work focuses on the use of HiSPoD to evaluate the effects of sample thickness and detector position on the acquisition and interpretability of collected diffraction patterns in an intensity-limited

experiment, with an example of the important of these considerations being provided by comparison of diffraction results for a metastable multi principal element alloy (MPEA) that exhibits phase transition during high-rate deformation.

2. Mitigating the diffraction effects of multiple harmonics by detector placement and sample geometry changes

2.1. Energy dependent beam attenuation as a result of heavy or thick samples

Undulators produce multiple peaks of intensity, referred to as harmonics, with higher order harmonics being associated with integer multiples of the peak energy of the first harmonic. Generally, these higher order harmonics less intense and broader than the first harmonic. An example energy spectrum from the U18 undulator (i.e. 1.8 cm period) at Sector 32-ID of the APS, and the energy spectrum used for all models and experiments in this work, is shown in Figure 1. These spectra can be simulated given information about the undulator and synchrotron in question; more details about the mechanics of undulators may be found in [1].

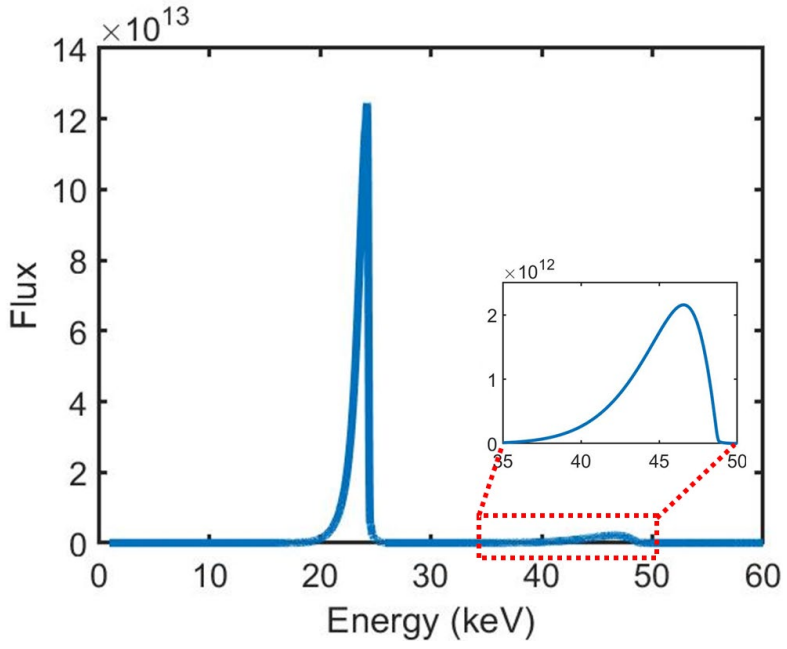

Figure 1 Example energy spectrum for a quasi-monochromatic beam at a synchrotron light source. This is produced by the undulator with 1.8 cm period at Sector 32-ID of the Advanced Photon Source with an undulator gap of 12 mm. All simulated diffraction and attenuated energy spectrum results in this work are generated using this spectrum.

As the X-ray diffraction of dynamic loading of materials often runs in transmission mode (a schematic of which is shown in **Figure 2**), the energy dependent absorption of X-rays, which favors transmission of higher energy X-rays can alter the relative intensities of peaks associated with different order harmonics. Low energy X-rays with lower penetration depths will have reduced diffracted intensity in thick samples, because the X-rays diffracted near the surface of the sample are unable to transmit through the rest of the sample without experiencing a second scattering event or being absorbed by the sample. Because higher level harmonics are higher in energy, they are less attenuated during transmission through the sample. Attenuation can be evaluated using the Beer-Lambert Law, which describes the transmitted intensity through a medium as a fraction of initial intensity determined by an exponential factor based on the distance travelled through the medium and a material dependent factor. The Beer-Lambert law is given below:

$$I = I_0 * e^{-x\,\mu(E)}$$

where x is the path length a photon must travel through the material and μ is the linear absorption coefficient, a material and photon energy dependent parameter that describes the absorption of incident photons [8]. A high μ results in lower transmitted intensity. Except near absorption edges of the element in question, μ decreases with increasing photon energy, and increases with increasing atomic number. Density normalized values of μ for elemental media are readily available from the National Institute for Standards and Technology (NIST) for a wide range of photon energies, and values for μ for alloys and compounds can be generated by taking an average of the μ for the components, weighted by their mass fraction [9]. Depending on alloy composition and thickness, this can result in the second harmonic producing higher diffracted intensities, relative to the first harmonic. An example of alloy and thickness effects on the relative intensities of the first and second harmonic and the associated effects on area diffraction patterns are shown in **Figure 3**.

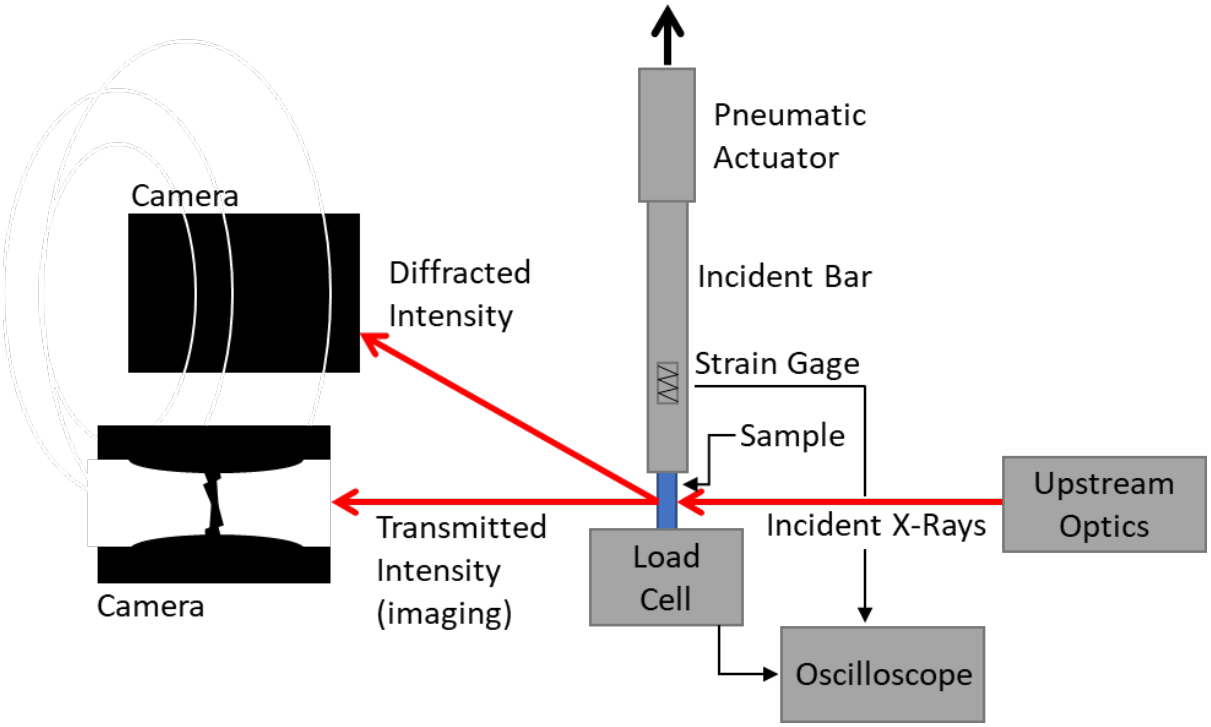

Figure 2 Schematic of the experimental setup for dynamic strain rate experiments at sector 32-ID of the APS, showing the positioning of the sample and detectors relative to the incident beam. Due to the requirement of the diffracted intensity to be transmitted through the sample in order to be collected, sample thickness effects become important for the diffraction.

Having too low a ratio of the first to second harmonic intensities can be deleterious to collected diffraction results; because the second harmonic is at a higher energy, the resulting rings will be closer to the beam center, as well as closer together, according to Bragg's Law. Considering the first and second harmonics, the peaks associated with the second harmonic will be at approximately one half the 2θ of their equivalent peak associated with the first harmonic. It then follows that peak separation for the second harmonic peaks is decreased by an approximate factor of two. This relationship works best for considering peaks at relatively low 2θ for the first harmonic as at higher 2θ, the approximation that $\sin(x) \approx x$ deteriorates. Additionally, because the second harmonic is broader, the resulting peaks will also be broad. The degree to which the second harmonic is broader will depend on beamline specific hardware and is difficult to generalize. The combination of peaks with reduced separation and increased broadness can result in peak overlap that is difficult to deconvolute. As a result, second harmonic peaks are not well suited for diffraction applications. The simulated diffraction patterns in Figure 3 to help illustrate

this show only peak broadening due to the polychromatic nature of the incident beam and the effect of attenuation of the beam on the relative intensities of the harmonics. These patterns are generated in HiSPoD by defining a detector (using parameters sample to detector distance, detector angle, pixel size, image size, direct beam X and direct beam Y), providing a energy spectrum as a text file, and applying an absorption correction based on a user generated text file. The resulting simulated diffraction does not include peak broadening as a result of full-field diffraction occurring at multiple locations within the volume of the sample, small crystallites, strain distribution, or the noise inherent to high-rate testing, only the broadening from the polychromatic nature of the beam.

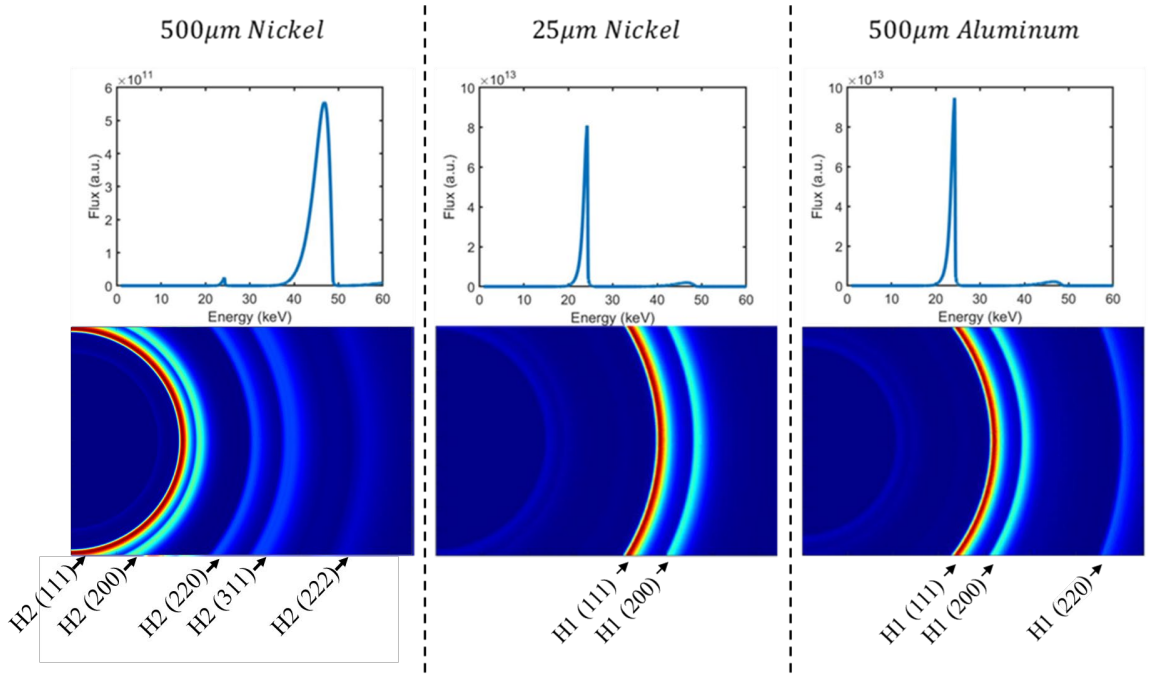

Figure 3 Attenuation corrected energy spectrums and simulated diffraction patterns of various thicknesses of pure Al and Ni, highlighting the effect of composition and thickness on the relative intensity of the first and second harmonics. The most intense peaks are indexed; those associated with the first harmonic are labelled as H1 and peaks associated with the second harmonic are labelled as H2. For the case of the 500 μm Ni there is overlap of the H1 (111) with H2 (222) and H1 (200) with H2 (400). The H1 (220) peak is visible in the Al case because, while Al and Ni share the same crystal structure, FCC, Al has a larger lattice parameter. The parameters describing detector position are listed in **Table 2** under Position 1.

Light metals, like aluminum (Al), have low attenuation coefficients and thus higher intensities for the peaks associated with the lower energy first harmonic. Heavier metals, such as nickel (Ni), have higher attenuation coefficients and thus lower relative intensities for the lower energy first harmonic. This effect can be mitigated by using a thinner sample. Practical limits exist, however. Heavier metals, such as Ni, may require very thin samples to avoid attenuating the first harmonic significantly. If, for an experiment, it were desired that a Ni sample have the same relative height of the first and second harmonics as does a 500 μm Al, sample, the nickel sample would have to be less than 25 μm in thickness (**Figure 3**). Sample this thin may be beyond a practical limit for machining or use. While the minimum thickness that can be experimentally useful will vary by experiment, having very thin samples introduces concerns about the size of the grains relative to the sample. Note also for the case of the $500\ \mu m$ thick Ni sample that the peaks associated with the second harmonic are closer together and broader as compared to their equivalent peaks in the $25\ \mu m$ Ni or $500\ \mu m$ Al first harmonic cases.

2.2. Detector positioning to minimize unavoidable second harmonic effects

In cases where second harmonic effects cannot be mitigated by thinning of the sample, the second harmonic may be avoided by moving the high intensity peaks associated with it out of the frame of view of the diffraction camera, so a longer detector gating time can be used for improving the signal-to-noise ratio of the data. This idea is explored in **Figure 4**. When the high intensity peaks associated with the second harmonic are moved out of the view of the camera, as in position 2, the highest intensity peak associated with the first harmonic becomes the maximum intensity against which other peaks present are normalized in processing. The high (hkl) index peaks associated with the second harmonic may still be in view of the camera; however, they are likely to have lower relative intensities. Consequently, more peaks associated with the first harmonic are now visible. Identifying the peaks associated with the first and second harmonic is possible through use of the "Label (hkl) in I(tth)" function of HiSPoD.

There are limits to this technique. As the detector is rotated away from the beam center, the fraction of each new ring falling within the view of the camera is decreased, and thus the absolute diffracted intensity collected for these rings falls. If the absolute intensity is too low, these rings may become unobservable against noise. Moving the detector closer to the sample can combat this by increasing the fraction of the ring in view of the camera. Moving the detector

closer will also have the effect of increasing the range of 2θ sampled, but the reciprocal space resolution is compromised as the diffraction rings get closer. This is explored by position 3 in **Figure 4.** The ideal detector position is also impacted by several detector parameters, most notably the detector's area and pixel size. Large area detectors provide several obvious benefits to diffraction experiments, allowing either capture of a larger azimuthal range (a larger fraction of each ring) or a wider reciprocal-space range at a given sample to detector distance. Similarly, the pixel size can affect reciprocal-space resolution, with smaller pixels producing a better reciprocal-space resolution. This enables a detector with a smaller pixel size to be placed closer to the sample while maintaining the same reciprocal-space resolution. Hardware alternatives to moving the detector can allow for the effects of the higher order harmonics to be mitigated, but may be more complicated than moving the detector, especially if only a small shift is required to avoid capturing the higher order peaks. These hardware solutions may include different types of slits or masks on the detector. The difficulties associated with hardware solutions involve the positioning of them in such a way as to eliminate only the undesirable peaks as well as the non-uniqueness of masks for the detector, where different materials and different detector positions may different masks.

In practice, it will likely be simpler to use HiSPoD to find the best experimental parameters for the phase transition of a material one wishes to observe, and then simulate the pattern of Al or another reference material using the same experimental parameters. Setting up for experiments at a light source, one can then move the detector into such a position that the collected pattern matches the desired simulated pattern for the reference. Any fine-grained, light metal would produce satisfactory results. Al foil is a readily available and effective reference material. An additional reference material with similar structure and lattice parameter the material of interest may also be of use for positioning the beam if the sample does not produce clear diffraction patterns. This method is superior to using the parameters (i.e. Sample-to-Detector, Detector Angle, Direct Beam X, Direct Beam Y) entered in the "Experiment Parameters" portion of the HiSPoD graphical user interface as a guide to positioning the diffraction camera, as several of the experimental parameters are compounded by optics, especially the sample to detector distance.

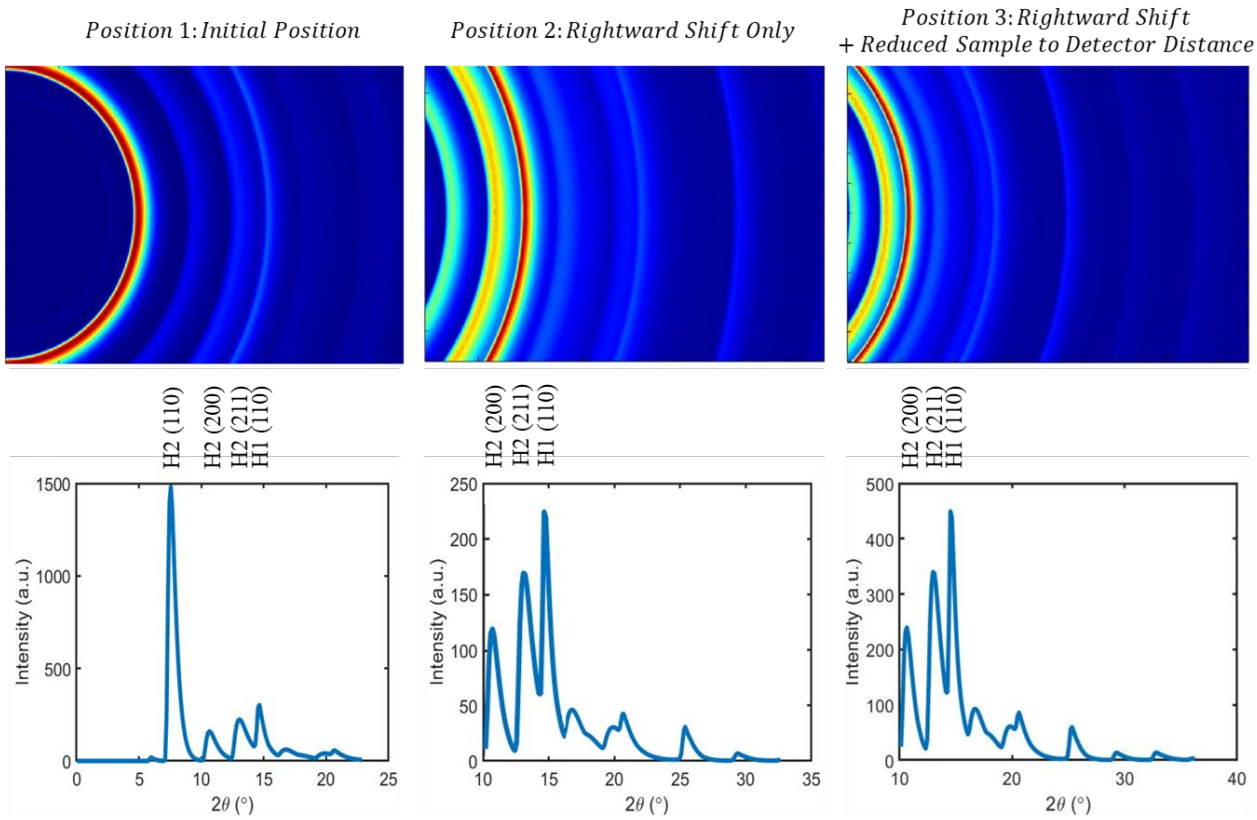

Figure 4 Simulated area diffraction patterns and corresponding integrated I vs 2θ plots for a 500 μm thick iron sample, illustrating how shifting the detector position can alter collected diffraction patterns. The most intense peaks are indexed for each integrated I vs 2θ plot; the first and second harmonic peaks are labelled as H1 and H2, respectively. The parameters used to generate these simulated diffraction patterns are listed in **Table** 1. Note that different scales are used for intensity on each integrated plot

Table 1 Parameters used to simulate diffraction patterns in **Figures 3** and **4.** For all cases, Detector angle is 0, scaling factor is 1 and the number of harmonics is 2. 2θ range is a result of the parameter choices and is not an input.

Position	Sample-to-detector (mm)	Direct Beam-X (pix.)	Direct Beam-Y (pix.)	Image Dim. (pix.)	Pixel Size (um)	Detector Angle (°)	2θ Range (°)
1	60	0	250	500*750	32	0	0-23

2	60	-300	250	500*750	32	0	10-33
3	45	-300	250	500*750	32	0	10-36

While the second harmonic remains more intense than the first for all cases in **Figure 4**, for lateral-shifted camera positions in positions 2 and 3, the only visible peaks associated with the high intensity second harmonic are high index peaks with relatively low diffracted intensities. This enables observation of peaks that would have been too low in relative intensity to be observed simultaneously with the low index second harmonic peaks. Because the most intense peak is now associated with the first harmonic, other first harmonic peaks have relative intensity equal to that expected if the second harmonic were not considered. Because the first harmonic peaks are low in absolute intensity due to the sample absorption, moving the detector closer to the sample can result in increased collected intensity, as more of each ring is in the view of the camera; additionally, this reduces scattering by the air between the sample and the detector. However, this also results in decreasing the separation between peaks, as shown by position 3. As an alternative, the highest intensity second harmonic peaks may be masked after the fact, though this reduces the 2θ range measurable. If the detector is not moved laterally, then the detectors dynamic range becomes important. A detector with high dynamic range will allow the collection of the relatively low intensity first-harmonic peaks while still collecting intensity information from the higher intensity second-harmonic peaks, which can then be masked or referenced in the post processing. A detector with lower dynamic range may saturate the highest intensity second-harmonic peaks before enough signal is collected from the first-harmonic peaks to be of sufficient quality. Depending on the detector, saturation may not be an issue and the saturated regions can simply be masked, however; large, saturated areas may result in altered backgrounds or other artifacts.

In cases where the first harmonic does not provide sufficient intensity, even at the limit of feasibility for thinning the sample, the second harmonic may be preferable. In these instances, which may apply in materials like steels or other strongly absorbing materials, reciprocal-space resolution may be gained by moving the detector away from the sample, but at the expense of the fraction of each ring captured on the detector.

3. Application of HiSPoD based experimental geometry planningto a $Co_{50}Cr_{40}Ni_{10}$ MPEA

3.1. A brief description of TRIP behavior and interest

In-situ X-ray diffraction experiments are greatly beneficial for transformation induced plasticity (TRIP) enabled alloys as a means of observing the correlation between strain and transformation progress [10–12]. Alloys with TRIP behavior are of particular interest as structural materials, as TRIP behavior results in increased work hardening rates, delaying instability and producing increased ultimate tensile strength and uniform elongation [13]. Thus, TRIP enabled MPEAs hold promise as blast resistant materials, necessitating the study of their TRIP behavior from quasi-static to dynamic rates. At quasi-static strain rates, these experiments may be performed at a wide range of user facilities with monochromatic beams, because these are not intensity limited experiments. Interrupted testing or magnetic measurements may also allow similar studies without the need for a synchrotron light source [14–17], but light source experiments afford deeper insights into when phase transformation occurs during deformation.

For experiments at higher strain rates, intensity becomes a limiting factor in the time-resolution of the diffraction, especially as many TRIP alloys are Fe-, Mn-, Ni-, or Co-rich, and thus have high X-ray attenuation coefficients [13, 18]. The use of polychromatic beams to overcome this limitation can obscure changes in the diffraction, such as the appearance of new peaks due to a phase transition. To overcome the effect of the polychromatic nature of the incident beam used in these experiments, the techniques discussed above were applied to an FCC→HCP TRIP enabled $Co_{50}Cr_{40}Ni_{10}$ alloy.

3.2. Second Harmonic Effects in $Co_{50}Cr_{40}Ni_{10}$

The first harmonic peak intensity of the incident beam used lies at 24.23 keV ($\lambda = 0.5117\dot{A}$) and has an associated mass attenuation coefficient in Co of $143.6\ \mathrm{cm}^{-1}$, in Cr of $84.2\ \mathrm{cm}^{-1}$, and in Ni of $166.1\ \mathrm{cm}^{-1}$. The second harmonic peak intensity at 46.82 keV ($\lambda = 0.2648$ Å) has attenuation coefficients of $22.5\ \mathrm{cm}^{-1}$ in Co, $12.9\ \mathrm{cm}^{-1}$ in Cr and $26.3\ \mathrm{cm}^{-1}$ in Ni. As the attenuation coefficients are much larger for the energy of the first harmonic as compared to the second harmonic, it can be anticipated that there are substantial changes in the relative intensity of the first and second harmonic for thick samples of this material. A quantitative assessment of this is shown in **Figure 5,** which shows the attenuation corrected energy spectra for two thicknesses of $Co_{50}Cr_{40}Ni_{10}$. While true optimization is not supported by

HiSPoD, sample thickness and detector position may be iterated to arrive at improved experimental geometries.

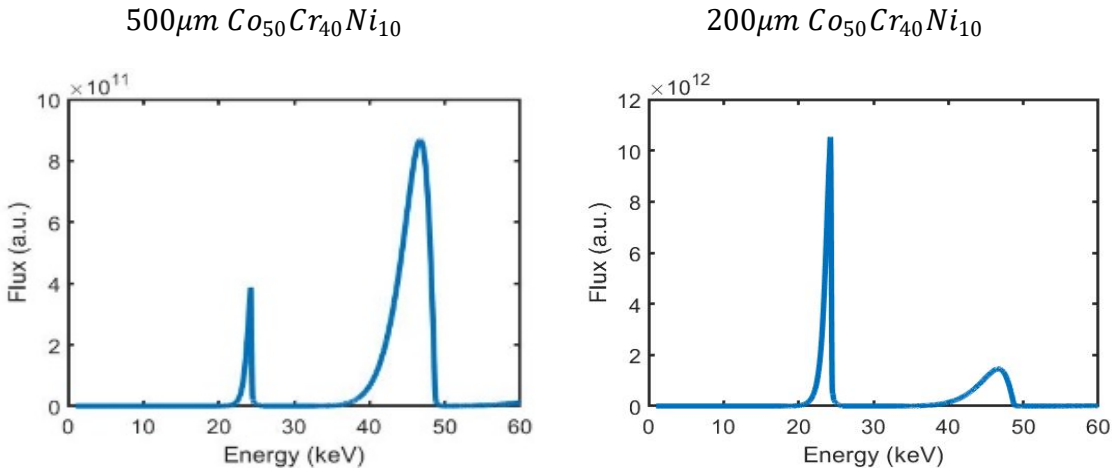

Figure 5 Attenuation corrected energy spectra for given thicknesses of a TRIP enabled CoCrNi MPEA. As thickness decreases, both the relative intensity of the first and second harmonics and the absolute transmitted intensity increases. These thicknesses correspond to sample thicknesses used during experiments at beamline 32-ID of the APS.

3.3. Simulations of Phase Transformation Compared to Experimental Results

These energy spectra can be used to enable comparisons between individual simulated area diffraction patterns for $Co_{50}Cr_{40}Ni_{10}$, which are explored in **Figure 6**, illustrating the importance of sample position and thickness. Additionally, attenuation corrected energy spectra can be used to generate simulations of the transformation within HiSPoD, using its built-in simulation functions. This involves simulating the area pattern for a range of phase fractions, then using HiSPoD to process the simulated patterns again to generate "heatmaps" of 2θ vs. Intensity vs. fraction transformed. These simulations are useful for both identifying preferable detector positions for observing a given phase transformation, and also for qualitative comparisons with experimental results of the extent of transformation. This is explored in **Figure 7** for the example FCC→HCP TRIP alloy. TRIP behavior is readily observed in the HiSPoD iterated pattern, while it is difficult to identify in the intial case. Relative to the initial case, the iterated case uses thinner samples (100 μm vs 500 μm) and experiences a lateral detector shift, as well as reduced sample to detector distance.

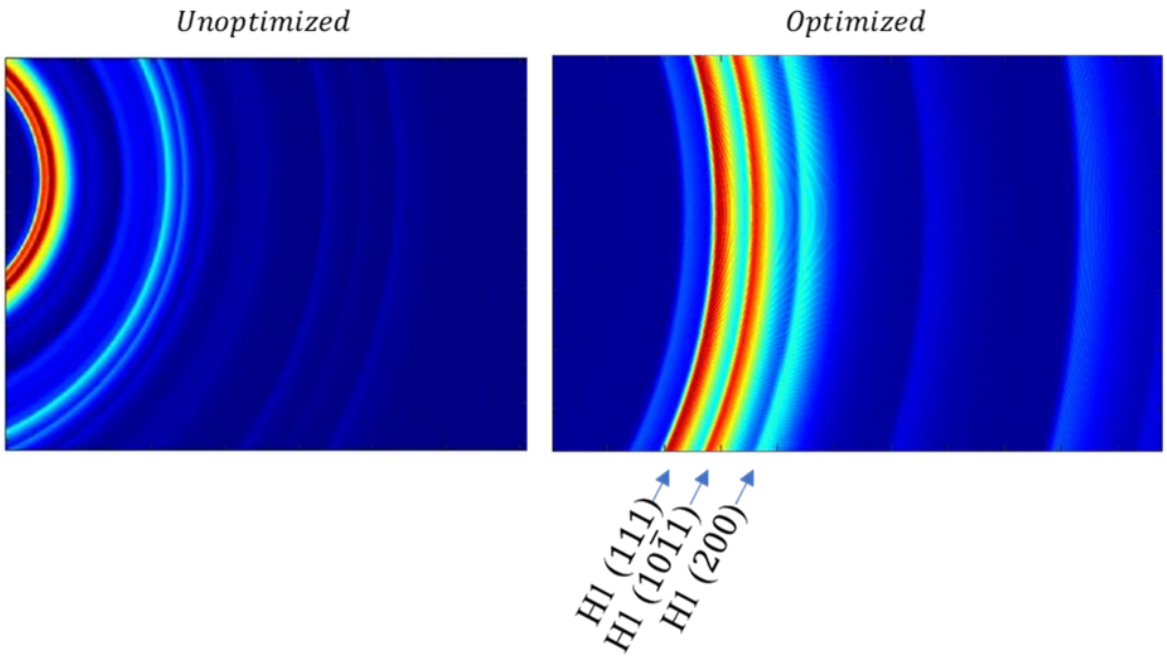

Figure 6 Simulated optimized and unoptimized area diffraction patterns for a 50/50 mixture of FCC and HCP phases in $Co_{50}Cr_{40}Ni_{10}$ tested during high strain rate deformation at beamline 32-ID-B of the APS. The highest intensity peaks for the optimized case are indexed. Due to the overlapping of the peaks in the initial case, individual peaks are difficult to identify. Differences between the aspect ratio of the experimental patterns are a result of different diffraction cameras used during the different experiments the optimized and unoptimized simulations are meant to represent, see details in text.

Table 2 Parameters used to simulate diffraction patterns in **Figure 6.** For all cases scaling factor is 1 and the number of harmonics is 2. 2θ range is a result of the parameter choices and is not an input.

Position	Sample-to-detector (mm)	Detector Angle (°)	Direct Beam-X (pix.)	Direct Beam-Y (pix.)	Image Dim. (pix.)	Pixel Size (um)	2θ Range (°)
Intitial	70	20	-165	150	512*712	50	5-38
Iterated w/ HiSPoD	44	3	-240	100	250*400	32	10-26

Some differences exist between the experimental area diffraction results that are not attributable to the differences in sample thickness and detector position. These include a difference in aspect ratio and the presence of a ring of anomalous intensity near the edges of the unoptimized condition. These differences are a result of a difference in the camera-scintillator set-up used in the experiments, as the patterns were collected during two separate visits to the APS. Optimized patterns were collected using a Shimadzu Hyper-Vision HPV-X2 camera, while the unoptimized patterns were collected using a Photron FASTCAM SA1.1. In addition to the differences mentioned above, the Shimadzu camera is also capable of recording at a higher frame and resolution.

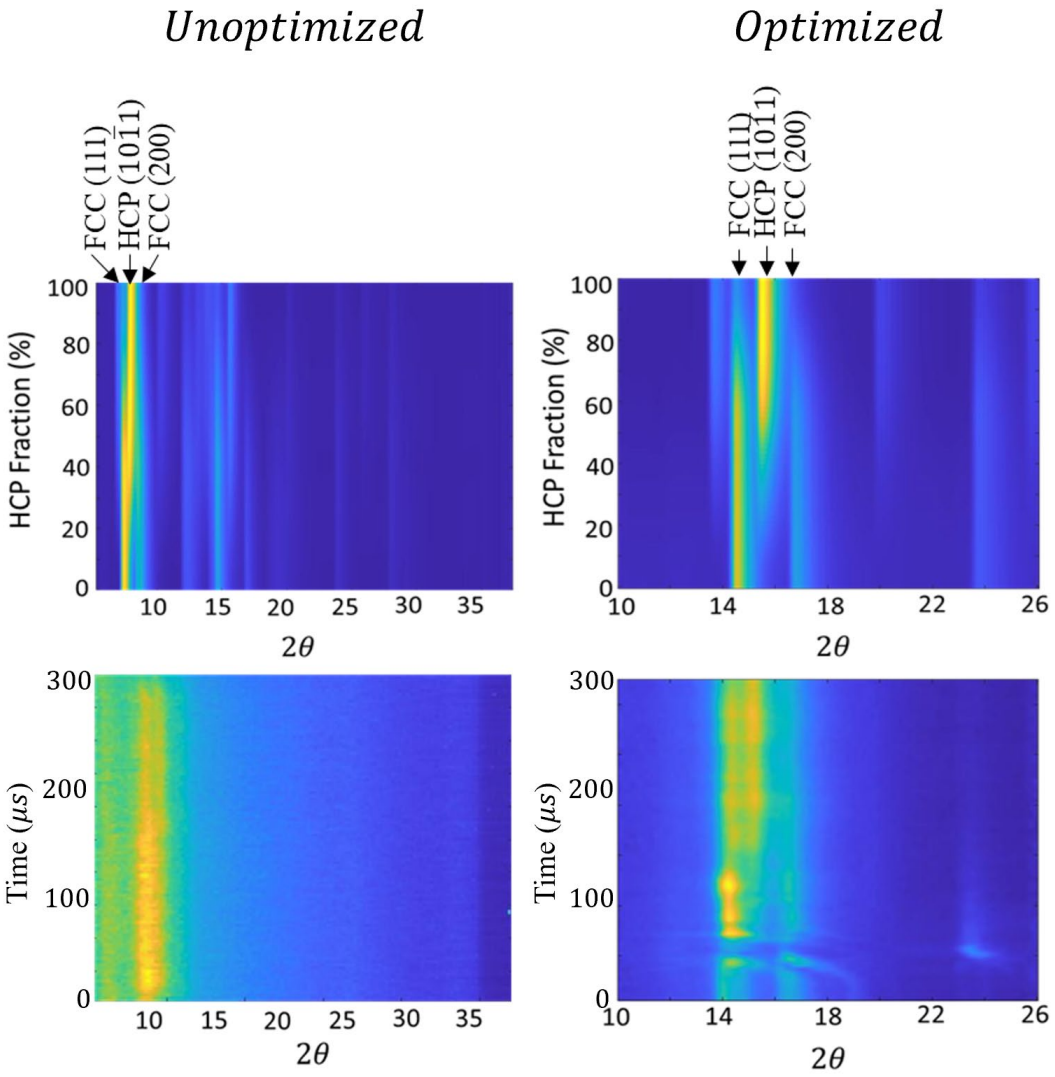

Figure 7 (Top) A comparison of an initial and iterated simulation of complete FCC→HCP transformation in $Co_{50}Cr_{40}Ni_{10,}$ as well as (bottom) experimental results. In these simulations, the decrease in intensity of the FCC $\{111\}$ and $\{200\}$ peaks and appearance of the HCP $\{10\bar{1}1\}$ peak are much more evident in the optimized case, which uses both a decreased sample thickness ($100\ \mu m$ vs. $500\ \mu m$), decreased sample to detector distance and lateral shift in detector position. In the initial case, the high intensity of the high energy second harmonic results in the evidence of transformation being obscured by overlapping, broad peaks that are difficult to deconvolute, and the low intensity of peaks with sufficient separation to distinguish. In the iterated case, evidence of the transformation is clearer, as the peaks are both sharper and have greater separation. Several peaks in the initial case are visible in the simulated diffraction that not in the experimentally observed patterns. This is due to the high background inherent to high-rate experiments, which may cause low intensity peaks to be obscured by noise.

4. Summary

Access to synchrotron light sources is generally limited, and users are often unable to make significant changes to their samples during their allotted beamtime. As a result, efforts must be made to ensure optimal experimental results are obtained. To this end, HiSPoD can serve as a powerful tool, not just for the post-processing of data collected during experiments at a beamline, but also for preparatory work. HiSPoD's ability to modulate the incident energy spectrum by energy dependent attenuation allows for determination of sample thicknesses that improve relative intensities of the various harmonics produced by undulators. This is especially important for observation of phase transitions in materials such as TRIP steels or MPEAs, where high attenuation coefficients result in low diffracted intensities for the sharp first harmonic and low attenuation for the higher energy, but broad second harmonic. Beyond sample thickness effects, HiSPoD's simulation capabilities allow for identification of preferable detector positions to further mitigate effects of the second harmonic. As illustrated by the comparison between the unoptimized and optimized diffraction results presented in **Figure 7,** these methods have been used to improve the in-situ study of phase transition in $Co_{50}Cr_{40}Ni_{10}$ with synchrotron X-ray diffraction using a polychromatic beam during high strain rate testing.

5. References

1. Ternov IM (1995) Synchrotron radiation. Physics-Uspekhi 38:409–434. https://doi.org/10.1070/PU1995v038n04ABEH000082

2. Navirian H, Shayduk R, Leitenberger W, et al (2012) Synchrotron-based ultrafast x-ray diffraction at high repetition rates. Review of Scientific Instruments 83:063303

3. Wang B, Tan D, Lee TL, et al (2018) Ultrafast synchrotron X-ray imaging studies of microstructure fragmentation in solidification under ultrasound. Acta Materialia 144:505–515. https://doi.org/10.1016/j.actamat.2017.10.067

4. Caciuffo R, Melone S, Rustichelli F, Boeuf A (1987) Monochromators for x-ray synchrotron radiation. Physics Reports 152:1–71

5. Sun T, Fezzaa K (2016) HiSPoD: A program for high-speed polychromatic X-ray diffraction experiments and data analysis on polycrystalline samples. Journal of Synchrotron Radiation 23:1046–1053. https://doi.org/10.1107/S1600577516005804

6. Hudspeth M, Claus B, Dubelman S, et al (2013) High speed synchrotron x-ray phase contrast imaging of dynamic material response to split Hopkinson bar loading. In: Review of Scientific Instruments. American Institute of PhysicsAIP, p 025102

7. Luo SN, Jensen BJ, Hooks DE, et al (2012) Gas gun shock experiments with single-pulse x-ray phase contrast imaging and diffraction at the Advanced Photon Source. Review of Scientific Instruments 83:073903

8. Swinehart DF (1962) The Beer-Lambert Law. Journal of Chemical Education 39:333–335

9. Hubbell JH, Seltzer SM (2004) Tables of X-Ray Mass Attenuation Coefficients and Mass Energy-Absorption Coefficients from 1 keV to 20 MeV for Elements Z = 1 to 92 and 48 Additional Substances of Dosimetric Interest*. In: Radiation Physics Division, PML, NIST

10. Coury FG, Santana D, Guo Y, et al (2019) Design and in-situ characterization of a strong and ductile co-rich multicomponent alloy with transformation induced plasticity. Scripta Materialia 173:70–74. https://doi.org/10.1016/j.scriptamat.2019.07.045

11. Fu B, Yang WY, Wang YD, et al (2014) Micromechanical behavior of TRIP-assisted multiphase steels studied with in situ high-energy X-ray diffraction. Acta Materialia 76:342–354. https://doi.org/10.1016/j.actamat.2014.05.029

12. Li N, Wang YD, Liu WJ, et al (2014) In situ X-ray microdiffraction study of deformation-induced phase transformation in 304 austenitic stainless steel. Acta Materialia 64:12–23. https://doi.org/10.1016/j.actamat.2013.11.001

13. Liu L, He B, Huang M (2018) The Role of Transformation-Induced Plasticity in the Development of Advanced High Strength Steels. Advanced Engineering Materials 20:1701083. https://doi.org/10.1002/adem.201701083

14. Yan K, Liss KD, Timokhina IB, Pereloma E V. (2016) In situ synchrotron X-ray diffraction studies of the effect of microstructure on tensile behavior and retained austenite stability of thermo-mechanically processed transformation induced plasticity steel. Materials Science and Engineering A 662:185–197. https://doi.org/10.1016/j.msea.2016.03.048

15. Tian Y, Lin S, Ko JYP, et al (2018) Micromechanics and microstructure evolution during in situ uniaxial tensile loading of TRIP-assisted duplex stainless steels. Materials Science and Engineering A 734:281–290. https://doi.org/10.1016/j.msea.2018.07.040

16. Kaoumi D, Liu J (2018) Deformation induced martensitic transformation in 304 austenitic stainless steel: In-situ vs. ex-situ transmission electron microscopy characterization. Materials Science and Engineering A 715:73–82. https://doi.org/10.1016/j.msea.2017.12.036

17. Hecker SS, Stout MG, Staudhammer KP, Smith JL (1982) Effects of Strain State and Strain Rate on Deformation-Induced Transformation in 304 Stainless Steel: Part I. Magnetic Measurements and Mechanical Behavior. Metallurgical Transactions A 13:619–626. https://doi.org/10.1007/BF02644427

18. Wei S, He F, Tasan CC (2018) Metastability in high-entropy alloys: A review. Journal of Materials Research 33:2924–2937